

PAPER • OPEN ACCESS

## Non-local effects on travelling waves arising in a moving-boundary reaction–diffusion model

To cite this article: Nabil T Fadai and John Billingham 2022 *J. Phys. A: Math. Theor.* **55** 405701

View the [article online](#) for updates and enhancements.

You may also like

- [Rotating black holes in Einstein-aether theory](#)  
Alexander Adam, Pau Figueras, Ted Jacobson et al.
- [Numerical ultrasonic full waveform inversion \(FWI\) for complex structures in coupled 2D solid/fluid media](#)  
Jiaze He, Jing Rao, Jacob D Fleming et al.
- [Semi-infinite travelling waves arising in a general reaction–diffusion Stefan model](#)  
Nabil T Fadai



**IOP | ebooks™**

Bringing together innovative digital publishing with leading authors from the global scientific community.

Start exploring the collection—download the first chapter of every title for free.

# Non-local effects on travelling waves arising in a moving-boundary reaction–diffusion model

Nabil T Fadai\*  and John Billingham 

School of Mathematical Sciences, University of Nottingham, Nottingham NG7 2RD, United Kingdom

E-mail: [nabil.fadai@nottingham.ac.uk](mailto:nabil.fadai@nottingham.ac.uk)

Received 12 April 2022, revised 10 August 2022

Accepted for publication 1 September 2022

Published 19 September 2022



CrossMark

## Abstract

We examine travelling wave solutions of the partial differential equation  $u_t = u_{xx} + u(1 - u * \phi)$  on a moving domain  $x \leq L(t)$ , where  $u * \phi$  is the spatial convolution of the population density with a kernel  $\phi(y)$ . We provide asymptotic approximations of the resulting travelling waves in various asymptotic limits of the wavespeed, the non-local interaction strength, and the moving boundary condition. Crucially, we find that when the moving boundary has a weak interactive strength with the population density flux, there can be two different travelling wave solutions that move at the same wavespeed.

Keywords: Fisher's equation, non-local differential equation, Stefan condition, moving boundary problem

(Some figures may appear in colour only in the online journal)

## 1. Introduction

Travelling waves arise in a wide range of reaction–diffusion models [1–13], whereby the concentration of a particular species,  $u(x, t)$  moves across the one-dimensional domain  $x \in \mathbb{R}$  at a constant wavespeed  $c$  for time  $t > 0$ . One of the most commonly employed reaction–diffusion model that exhibits travelling waves is the FKPP model [2]:

$$u_t = u_{xx} + u(1 - u), \quad -\infty < x < \infty.$$

\*Author to whom any correspondence should be addressed.



Original content from this work may be used under the terms of the [Creative Commons Attribution 4.0 licence](https://creativecommons.org/licenses/by/4.0/). Any further distribution of this work must maintain attribution to the author(s) and the title of the work, journal citation and DOI.

This reaction–diffusion model, which we will refer to as the *diffusive logistic model* for neutrality [8], combines logistic growth with linear diffusion and exhibits travelling wave solutions with a wavespeed  $c \geq 2$  [1]. The speed of the associated travelling wave is unique and exclusively depends on the choice of the initial conditions.

More recently, there has also been particular interest in extending the diffusive logistic model with new model elements. For instance, one modification that has been made is to consider travelling waves that evolve behind a *moving boundary* instead of on the entire real line [7–11]:

$$u_t = u_{xx} + u(1 - u), \quad -\infty < x \leq L(t).$$

Here, the moving boundary  $L(t)$  moves at a speed proportional to the population flux at the edge of the travelling wave. This model extension gives rise to sharp-fronted semi-infinite travelling waves [7–11, 13] that exist for wavespeeds  $c \in [0, 2)$ . The incorporation of a sharp-fronted travelling wave is particularly appealing to applications in mathematical biology, in which the ‘edge’ of a moving population is known to be at a finite position in time [9–11]. Another recent extension of the diffusive logistic model is the incorporation of a non-local reaction term [12]:

$$u_t = u_{xx} + u(1 - u * \phi), \quad -\infty < x < \infty.$$

The non-local convolution operator,  $u * \phi$ , represents the influence of the non-local (i.e., global) interactions within a population. Based on the choice of the kernel  $\phi$ , the non-local diffusive logistic model can give rise to spatial patterning within a travelling wave and other non-monotone travelling waves [12], while the range of wavespeeds remains consistent with the diffusive logistic model:  $c \geq 2$ . While both extensions of the diffusive logistic model have their individual merits, the combination of a non-local diffusive logistic model with a moving boundary has yet to be considered.

In this work, we examine travelling wave solutions of a non-local diffusive logistic model with a moving boundary. We provide asymptotic approximations of the resulting travelling waves in various asymptotic limits of the wavespeed, the non-local interaction strength, and the moving boundary condition. Crucially, we find that when the moving boundary has a weak interactive strength with the population density flux, there can be two different travelling wave solutions that move at the same wavespeed.

## 2. The non-local moving-boundary model

We consider the non-dimensional partial differential equation (PDE) that describes the population density  $u(x, t)$  with a moving boundary condition at  $x = L(t)$ :

$$u_t = u_{xx} + u(1 - u * \phi), \quad -\infty < x < L(t), \tag{1}$$

$$\lim_{x \rightarrow -\infty} u(x, t) = 1, \quad u(L(t), t) = 0, \tag{2}$$

$$\dot{L}(t) = -\mu \partial_x u(x, t)|_{x \rightarrow L(t)^-}, \quad L(0) = L_0. \tag{3}$$

The moving boundary condition relates the speed of the moving front,  $\dot{L}(t)$ , to the concentration flux,  $-\partial_x u(x, t)$ , via the constant  $\mu > 0$ . The non-local operator,  $u * \phi$ , is defined as

$$u * \phi = \int_{-\infty}^{\frac{L-x}{\lambda}} \phi(y)u(x + \lambda y, t)dy = \frac{1}{\lambda} \int_{-\infty}^L \phi\left(\frac{\bar{y} - x}{\lambda}\right)u(\bar{y}, t)d\bar{y}, \quad \lambda > 0, \tag{4}$$

where the kernel  $\phi(x)$  is continuous, symmetric, positive, decreasing for  $x > 0$ , and normalised such that

$$\int_{-\infty}^{\infty} \phi(y)dy = 1, \tag{5}$$

so that we can expect solutions with  $u \rightarrow 1$  as  $x \rightarrow -\infty$ .

To examine the behaviour of travelling wave solutions of (1) with constant wavespeed  $c$ , which numerical solutions suggest are generated by positive initial conditions with sufficiently large compact support [9–11], we let  $u(x, t) = U(x - L_0 - ct) := U(z)$  and transform the PDE into an ordinary differential equation (ODE):

$$U''(z) + cU'(z) + U(z) \left[ 1 - \frac{1}{\lambda} \int_{-\infty}^0 \phi\left(\frac{\bar{y}-z}{\lambda}\right) U(\bar{y})d\bar{y} \right] = 0, \tag{6}$$

$$\lim_{z \rightarrow -\infty} U(z) = 1, \quad U(0) = 0, \quad U'(0) = -\frac{c}{\mu}. \tag{7}$$

The travelling wave coordinate  $z = x - L(t) = x - L_0 - ct$  is shifted in  $x$  by  $L_0$  so that it satisfies (3). Furthermore, by noting that the moving boundary and the travelling wave move at the same wavespeed, we have that  $\dot{L}(t) = c$  and therefore obtain the derivative condition stated in (7) by rearranging the moving boundary condition shown in (3).

### 2.1. Asymptotic analysis for $\lambda \ll 1$

If the non-local lengthscale is much smaller than the diffusion lengthscale, we have that  $\lambda \ll 1$ . In this case, we can construct an asymptotic approximation of the solution to (6) and (7) by performing a regular asymptotic expansion in powers of  $\varepsilon := \lambda^2$ :

$$U(z) \sim \sum_{n=0}^{\infty} \varepsilon^n U_n(z), \quad c \sim \sum_{n=0}^{\infty} \varepsilon^n c_n. \tag{8}$$

Noting that  $\phi(y)$  is an even function, we can expand the non-local operator  $U * \phi$  as

$$U * \phi \sim \sum_{n=0}^{\infty} \sum_{q=0}^n \varepsilon^n k_{2q} U_{n-q}^{(2q)}(z), \tag{9}$$

where

$$k_{2q} := \frac{1}{(2q)!} \int_{-\infty}^{\infty} \phi(y)y^{2q} dy \quad \text{and} \quad U_{n-q}^{(2q)}(z) = \frac{d^{2q}}{dz^{2q}} U_{n-q}(z). \tag{10}$$

It can therefore be shown that two-term asymptotic series can be constructed via the following ODEs:

$$\begin{aligned} O(1): \quad & U_0'' + c_0 U_0' + U_0(1 - U_0) = 0, \\ & \lim_{z \rightarrow -\infty} U_0(z) = 1, \quad U_0(0) = 0, \quad c_0 = -\mu U_0'(0), \end{aligned} \tag{11}$$

$$\begin{aligned} O(\varepsilon): \quad & \mathcal{L}[U_1] = -c_1 U_0' + k_2 U_0 U_0'', \\ & \lim_{z \rightarrow -\infty} U_1(z) = 0, \quad U_1(0) = 0, \quad c_1 = -\mu U_1'(0). \end{aligned} \tag{12}$$

Here, the linear operator  $\mathcal{L}[U_n] := U_n'' + c_0 U_n' + (1 - 2U_0)U_n$  persists at all powers of  $\varepsilon^n, n \geq 1$ . By taking an additional derivative of (11) with respect to  $z$ , it immediately follows that  $\mathcal{L}[U_0'] = 0$ , and hence  $U_0'$  is a homogeneous solution of  $\mathcal{L}[U_n] = 0$ . Thus, by introducing the change of variables  $U_1 = U_0' V_1$  and multiplying (12) by the integrating factor  $U_0' e^{c_0 z}$ , we have that (12) becomes

$$O(\varepsilon): \quad \left[ e^{c_0 z} (U_0')^2 V_1' \right]' = U_0' e^{c_0 z} [-c_1 U_0' + k_2 U_0 U_0''], \tag{13}$$

$$\lim_{z \rightarrow -\infty} U_1(z) = 0, \quad U_1(0) = 0, \quad c_1 = -\mu U_1'(0).$$

**2.1.1. Small- $\mu$  reduction.** In the small- $\lambda$  approximation of equations (6) and (7), we note that the leading-order approximation (11) reduces to the ‘Fisher–Stefan model’ (cf [9–11]). As shown in [9, 11], there is, in general, no analytical solution of (11) unless  $c_0 = 0$ . From (7), we expect that  $c \ll 1$  when  $\mu \ll 1$ , so we can make use of the analytical solution by considering the case  $\mu \ll 1$ . Specifically, we write  $\mu = \lambda^2 \hat{\mu}$ , in which case we expect  $c$  and  $\mu$  to be  $O(\lambda^2)$  as  $\lambda \rightarrow 0$ , i.e.  $c_0 = 0$ . In this limit, (11) becomes

$$U_0'' + U_0(1 - U_0) = 0, \tag{14}$$

$$\lim_{z \rightarrow -\infty} U_0(z) = 1, \quad U_0(0) = 0, \quad c_1 = -\hat{\mu} U_0'(0),$$

and can be solved by means of the first integral method:

$$U_0' = (U_0 - 1) \sqrt{\frac{2U_0 + 1}{3}}, \tag{15}$$

implying that

$$U_0(z) = 1 - \frac{3}{2} \operatorname{sech}^2[\theta(z)], \tag{16}$$

where

$$\theta(z) = \frac{z}{2} - \operatorname{sech}^{-1} \left( \sqrt{\frac{2}{3}} \right) = \frac{z - \log(2 + \sqrt{3})}{2}. \tag{17}$$

Next, the ODE for  $U_1(z)$  becomes

$$\mathcal{L}[U_1] = -c_1 U_0' + k_2 U_0 U_0'', \tag{18}$$

$$\lim_{z \rightarrow -\infty} U_1(z) = 0, \quad U_1(0) = 0, \quad c_2 = -\hat{\mu} U_1'(0).$$

By integrating twice and imposing the boundary conditions in (18), we obtain our correction term for  $\lambda \ll 1$ :

$$U_1(z) = -\frac{3}{4} \left[ \sqrt{3} k_2 - \frac{c_1(9 + 2\sqrt{3})}{5} + (c_1 - k_2)z \right] \tanh \theta \operatorname{sech}^2 \theta$$

$$- \frac{c_1}{10} \left[ (2 - \sqrt{3})e^z + 3(\tanh \theta + 1)(5 \tanh \theta - 3) \right] - \frac{3k_2}{16} \operatorname{sech}^2 \theta (10 - 9 \operatorname{sech}^2 \theta). \tag{19}$$

Furthermore, by evaluating the derivative conditions in (14) and (18), we find that

$$c_1 = \frac{\hat{\mu}}{\sqrt{3}}, \quad c_2 = \hat{\mu} \left( \frac{k_2}{4\sqrt{3}} - \frac{9 - 2\sqrt{3}}{15} \hat{\mu} \right), \tag{20}$$

implying that

$$c = \frac{\varepsilon \hat{\mu}}{\sqrt{3}} + \varepsilon^2 \hat{\mu} \left( \frac{k_2}{4\sqrt{3}} - \frac{9 - 2\sqrt{3}}{15} \hat{\mu} \right) + O(\varepsilon^3) = \frac{\mu}{\sqrt{3}} + \mu \left( \frac{\lambda^2 k_2}{4\sqrt{3}} - \frac{9 - 2\sqrt{3}}{15} \mu \right) + O(\lambda^6). \tag{21}$$

We also note that there is a critical value,  $\mu = \mu^*$ , with

$$\mu^* = \frac{5k_2\lambda^2}{12\sqrt{3} - 8} \approx 0.391k_2\lambda^2, \tag{22}$$

for which the correction to the wavespeed is  $O(\lambda^6)$ , not  $O(\lambda^4)$ .

*2.1.2. Comparison with small- $\mu$  asymptotic solutions of the Fisher–Stefan model.* In the previous subsection, we determined the small- $\mu$  asymptotic solution of the small- $\lambda$  regime of (6) and (7). In particular, the leading-order solutions of the non-local ODE and its local counterpart, with  $\mu \ll 1$ , sometimes referred to as the Fisher–Stefan model (cf [9–11]), are identical. It is therefore natural to compare the correction term of the asymptotic solution,  $U_1(z)$  shown in (19), with the correction term of the Fisher–Stefan model with  $\mu \ll 1$ . With reference to [9], the small-wavespeed asymptotic solution of the Fisher–Stefan model is determined by assuming that  $\mu \ll 1$ , as  $\lambda$  does not appear in the Fisher–Stefan model (and thus,  $k_2 = 0$ ). By expanding  $U(z)$  and the wavespeed  $c$  in terms of  $\mu$ ,

$$U(z) = U_0(z) + \mu U_1(z) + O(\mu^2), \quad c = c_1\mu + c_2\mu^2 + O(\mu^3), \tag{23}$$

we obtain the following ODEs:

$$O(1): \quad U_0'' + U_0(1 - U_0) = 0, \\ \lim_{z \rightarrow -\infty} U_0(z) = 1, \quad U_0(0) = 0, \quad c_1 = -U_0'(0), \tag{24}$$

$$O(\mu): \quad \mathcal{L}[U_1] = -c_1 U_0', \\ \lim_{z \rightarrow -\infty} U_1(z) = 0, \quad U_1(0) = 0, \quad c_2 = -U_1'(0). \tag{25}$$

By comparing (24) and (25) to (14) and (18), we confirm that the asymptotic approximation terms for  $U(z)$  in the non-local, small- $\mu$  model are identical to the small- $\mu$  Fisher–Stefan approximation terms with  $k_2 \equiv 0$  and  $\hat{\mu} = 1$ . We also note that the small- $\mu$  correction to travelling waves arising in the Fisher–Stefan model,  $U_1(z)$  in (25), has not been previously stated in the literature. However, we emphasise at this point that while the *terms* in each asymptotic approximation are identical, the asymptotic series themselves are different: (14) and (18) arise from asymptotic expansions in  $\lambda$  and  $\mu$ , while (24) and (25) arise from an asymptotic expansion in  $\mu$  alone.

### 3. Numerical solutions

In order to compare solutions of (6) and (7) with the asymptotic approximations developed above, we describe a simple numerical method for solving (6) and (7). Firstly, we truncate the domain of solution to  $-\ell \leq z \leq 0$ , with  $\ell > 0$ , and assuming that  $U = 1$  for  $z < -\ell$ . We therefore approximate the convolution term in (6) as

$$\frac{1}{\lambda} \int_{-\infty}^0 \phi\left(\frac{\bar{y}-z}{\lambda}\right) U(\bar{y}) d\bar{y} \approx \frac{1}{\lambda} \int_{-\infty}^{-\ell} \phi\left(\frac{\bar{y}-z}{\lambda}\right) d\bar{y} + \frac{1}{\lambda} \int_{-\ell}^0 \phi\left(\frac{\bar{y}-z}{\lambda}\right) U(\bar{y}) d\bar{y}. \tag{26}$$

For the remainder of this work, we will focus on two specific kernel functions:  $\phi(y) = \Phi_{\infty}(y)$  and  $\phi(y) = \Phi_1(y)$ , which are given by

$$\Phi_1(y) = \frac{1}{2} e^{-|y|}, \quad \Phi_{\infty}(y) = \frac{1}{2\sqrt{\pi}} e^{-\frac{1}{4}y^2}.$$

The notation for these kernels is chosen to be consistent with the notation introduced in [12]. For these two choices of kernels, the first integral in (26) can be computed analytically. Next, we discretize the domain of solution,  $-\ell \leq z \leq 0$ , at  $N$  equally-spaced points,  $z = z_i$  for  $i = 1, 2, \dots, N$ . All derivatives in (6) and (7) are evaluated using central finite differences. The second integral in (26) is evaluated using 16-point Gaussian quadrature for  $z_i \leq z \leq z_{i+1}$ , with  $U$  assumed to vary linearly between  $z = z_i$  and  $z = z_{i+1}$ . Numerical experiments suggest that this accurate representation of the kernel leads to greater accuracy in the solution for some kernels, and the overhead from using this many quadrature points is not excessive. The resulting set of nonlinear algebraic equations for the unknowns  $U(z_i)$  and  $c$ , for fixed values of  $\mu$  and  $\lambda$ , is solved using `fsolve` in MATLAB. Parameter continuation in  $(\mu, \lambda)$  space can then be used to explore the solution space.

Although unsteady solutions of initial value problems associated with (1)–(3) are not the main focus of the present paper, for completeness we also adapted the numerical scheme described above to study time-evolving solutions. In figure 1, the initial condition of  $U(x, 0) = 1 - e^x$  is used to mimic the qualitative features of a travelling wave, and Euler timestepping is used to update the solution. As is expected from similar analyses (see [9–11]), we see in figure 1 that the numerical solution approaches the travelling wave solution with no evidence of any temporal instability. Consequently, the interest of this non-local moving-boundary model continues to lie in the structure of the travelling wave solution and less in the evolution of a temporally unsteady solution.

#### 3.1. Comparison with small- $\lambda$ asymptotic solutions

Using the methods outlined above, we now compare the asymptotic approximations of the non-local moving-boundary model with numerical solutions. In particular, we note that for both choices of kernels,  $\Phi_1$  and  $\Phi_{\infty}$ , the second moment is  $k_2 = 1$  and therefore both two-term asymptotic approximations will be identical to one another. As such, we will focus on presenting comparisons between the asymptotic approximations and  $\phi = \Phi_1$  for the remainder of this section.

In figure 2(a), we compare the numerically-calculated solution and the leading order asymptotic approximation, shown in (16), for  $\lambda = 0.1$ . We see excellent agreement between the two

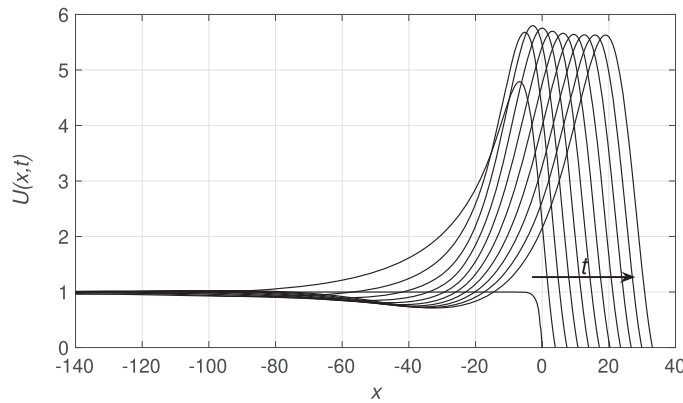


**Figure 1.** Numerical solution of the initial value problem (1)–(3), with  $\mu = 1$ ,  $\lambda = 100$ ,  $\phi = \Phi_1$ , and initial conditions  $U(x, 0) = 1 - e^{-x}$ ,  $L_0 = 0$ . The solution  $U(x, t)$ , shown at  $t = 0, 10, \dots, 100$ , tends to a stable travelling wave solution with constant wavespeed  $c \approx 0.3184$ .

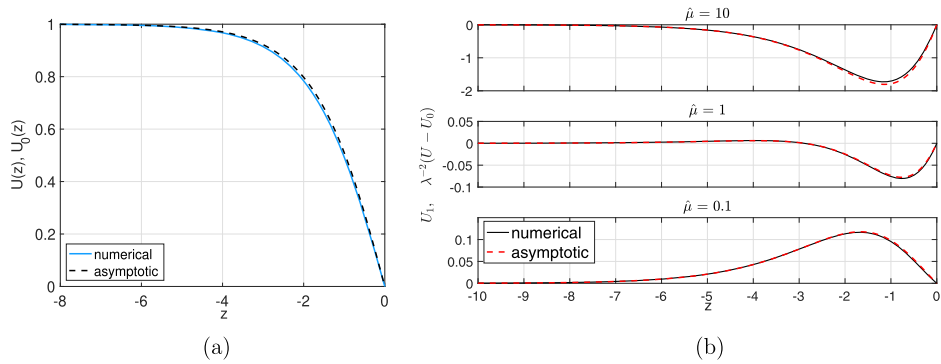


**Figure 2.** (a) Comparison of the asymptotic leading-order solution,  $U_0(z)$ , with the numerical solution for  $\hat{\mu} = 10$ ,  $\lambda = 0.1$ , and  $\phi = \Phi_1$ . Smaller values of  $\hat{\mu}$  have a stronger agreement with  $U_0(z)$ . (b) Comparison of the asymptotic correction term,  $U_1(z)$ , to the numerical solution correction term,  $\lambda^{-2}[U(z) - U_0(z)]$ , for  $\hat{\mu} = 0.1, 1$  and  $10$ .

solutions when  $\hat{\mu} = 10$ , and the agreement is even stronger for smaller values of  $\hat{\mu}$ . Additionally, we see in figure 2(b) that the agreement with the correction term in the asymptotic solution,  $U_1(z)$ , is also excellent.

We can also compare the numerically-calculated value of the wave speed,  $c$ , and the asymptotic expression (21) for small values of  $\lambda$  (figure 3). Again, we see excellent agreement for both  $\mu = \lambda^2$  and  $\mu = \mu^*$ , as given by (22). These numerical results confirm that the correction to the wavespeed approximation is  $O(\lambda^4)$  for  $\mu \neq \mu^*$  and  $O(\lambda^6)$  for  $\mu = \mu^*$ . When the correction to the leading-order expression is less than  $10^{-8}$  in absolute value, we cannot easily calculate a sufficiently accurate numerical solution for  $\lambda \ll 1$ . As such, any discrepancies appearing in figure 3 for very small values of  $\lambda$  are due to numerical error rather than the asymptotic approximations themselves.

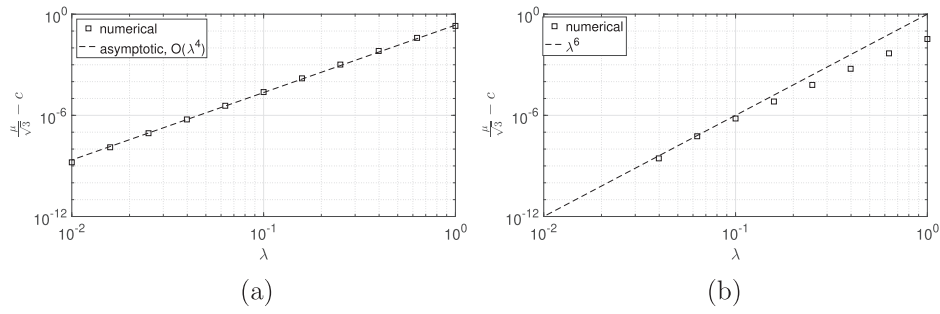


**Figure 3.** Comparison between the numerical and asymptotic calculations of the wavespeed correction (21) for (a)  $\mu = \lambda^2$  and (b)  $\mu = \mu^* \approx 0.391\lambda^2$ , as given by (22). Both figures use the kernel  $\phi = \Phi_1$ , for which  $k_2 = 1$ . Note that the broken line in (b),  $\lambda^6$ , is used to demonstrate that the correction to the wavespeed is  $O(\lambda^6)$ , as predicted by (21).

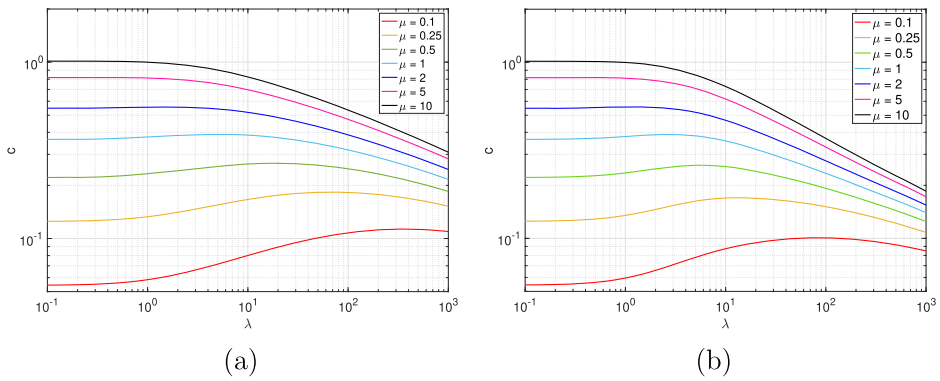


**Figure 4.** The numerically-calculated wavespeed  $c$  as a function of  $\lambda$  for various values of  $\mu$  and (a)  $\phi = \Phi_1$  (b)  $\phi = \Phi_\infty$ .

3.2. Solutions for larger  $\lambda$

We conclude by briefly presenting some numerical solutions for larger values of  $\lambda$ . As shown in [12], we expect that for  $\lambda \gg 1$ , the travelling wave profiles are strongly dependent on the choice of kernel; as such, we will consider the kernels  $\phi = \Phi_1$  and  $\phi = \Phi_\infty$  separately. In figure 4(a), we see that for the kernel  $\phi = \Phi_1$ , the wavespeed decreases monotonically as  $\lambda$  increases, for sufficiently large values of  $\mu$ , but for smaller values of  $\mu < 1$  the wavespeed has a maximum at some finite  $\lambda$ . This fact demonstrates for that smaller values of  $\mu$ , there are two values of  $\lambda$  that produce two different travelling wave profiles that move at the same wavespeed. For all values of  $\mu$  investigated, it would appear that  $c \rightarrow 0$  as  $\lambda \rightarrow \infty$ , with some (numerical) indication that  $\mu \approx O(\lambda^{-0.3})$ . While the  $c(\lambda, \mu)$  curves are different for the kernel  $\phi = \Phi_\infty$  (figure 4(b)), the aforementioned qualitative traits continue to hold.

While the influence of  $\lambda$  and  $\mu$  on the wavespeed provide similar qualitative traits for both kernels, the shape of the travelling waves themselves can vary drastically. As discussed in [12], linear theory can describe the oscillatory form of the far field as  $z \rightarrow -\infty$ . However, the formation of distinct spikes and their location is controlled by the regularity of the kernel at

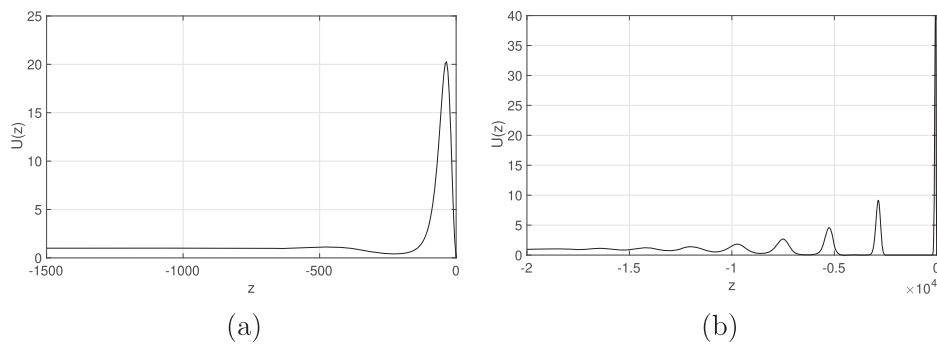


**Figure 5.** The travelling wave solution,  $U(z)$ , for  $\mu = 1$  and  $\lambda = 10^3$  for (a)  $\phi = \Phi_1$  (b)  $\phi = \Phi_\infty$ . Note that the axes in each subfigure differ from one another.

the origin in a highly non-trivial manner [12] and is beyond the scope of the present paper. With reference to figure 5, we note that for  $\lambda = 1000$  and  $\mu = 1$ , the kernel  $\phi = \Phi_1$  produces a travelling wave with a large maximum near  $z = 0$ , with oscillations rapidly decaying to the far-field condition of  $U = 1$ . Conversely, for the same value of  $\lambda$  and  $\mu$ , the kernel  $\phi = \Phi_\infty$  produces multiple spikes behind the wavefront. Both of these qualitative features are identical to those analysed for  $\lambda \gg 1$  in [12] for the infinite-domain version of this problem (i.e.,  $U \rightarrow 0$  as  $z \rightarrow \infty$ ). Indeed, the analysis of the structure of the solution proceeds in exactly the same way except close to  $z = 0$ , where we would need to apply the boundary conditions  $U = 0$  and  $U'(0) = -c/\mu$ .

While the modification of infinite travelling waves to semi-infinite travelling waves may seem minor, and that we should be able to find the full asymptotic solution of  $\lambda \gg 1$  as in [12], the situation is not as simple as it first appears. The first technical difficulty is that in the semi-infinite domain, the wavespeed associated with a particular travelling wave solution is determined globally; in contrast, for the infinite domain problem, the minimum wavespeed is  $c = 2$  and is determined locally in the same way as in the local diffusive logistic equation. This means that the asymptotic solution in the wavefront must be carefully matched to a solution valid up to  $z = 0$  to determine the leading-order wavespeed. This leads us to our second difficulty: unlike in [12], where a leading-order WKB approximation is sufficient to determine the (far-field) behaviour of the travelling wave's sequence of spikes, a two-term WKB approximation would now be required to satisfy the moving boundary condition at  $z = 0$ . In addition, it is apparent that the small-wavespeed behaviour for  $\lambda \rightarrow \infty$  does not emerge in any obvious way from the analysis presented in [12]. Due to these challenges, we leave the associated large- $\lambda$  asymptotic analysis for future consideration.

### Data availability statement

All data that support the findings of this study are included within the article.

### ORCID iDs

Nabil T Fadai  <https://orcid.org/0000-0001-7717-5421>

John Billingham  <https://orcid.org/0000-0002-4392-5770>

## References

- [1] Murray J D 2003 *Mathematical Biology I: An Introduction* (Berlin: Springer)
- [2] Fisher R A 1937 The wave of advance of advantageous genes *Ann. Eugenics* **7** 355–69
- [3] Aronson D G 1980 Density-dependent interaction-diffusion systems *Dynamics and Modelling of Reactive Systems* (Amsterdam: Elsevier) pp 161–76
- [4] Harris S 2004 Fisher equation with density-dependent diffusion: special solutions *J. Phys. A: Math. Gen.* **37** 6267
- [5] Gilding B H and Kersner R 2005 A Fisher/KPP-type equation with density-dependent diffusion and convection: travelling-wave solutions *J. Phys. A: Math. Gen.* **38** 3367
- [6] Wang D-S and Zhang Z-F 2008 On the integrability of the generalized Fisher-type nonlinear diffusion equations *J. Phys. A: Math. Theor.* **42** 035209
- [7] Bao W, Du Y, Lin Z and Zhu H 2018 Free boundary models for mosquito range movement driven by climate warming *J. Math. Biol.* **76** 841–75
- [8] Du Y and Lin Z 2010 Spreading-vanishing dichotomy in the diffusive logistic model with a free boundary *SIAM J. Math. Anal.* **42** 377–405
- [9] El-Hachem M, McCue S W, Jin W, Du Y and Simpson M J 2019 Revisiting the Fisher–Kolmogorov–Petrovsky–Piskunov equation to interpret the spreading-extinction dichotomy *Proc. R. Soc. A* **475** 20190378
- [10] Fadaï N T and Simpson M J 2020 New travelling wave solutions of the Porous–Fisher model with a moving boundary *J. Phys. A: Math. Theor.* **53** 095601
- [11] Fadaï N T 2021 Semi-infinite travelling waves arising in a general reaction–diffusion Stefan model *Nonlinearity* **34** 725
- [12] Billingham J 2020 Slow travelling wave solutions of the nonlocal Fisher-KPP equation *Nonlinearity* **33** 2106
- [13] Du Y 2022 Propagation and reaction–diffusion models with free boundaries *Bull. Math. Sci.* **12** 2230001